Experimental realization of a reconfigurable electroacoustic topological insulator

Amir Darabi[a], Manuel Collet[b], and Michael J. Leamy[a,1]

[a]Woodruff School of Mechanical Engineering, Georgia Institute of Technology, Atlanta, GA 30318; and [b]Laboratory of Tribology and System Dynamics, UMR CNRS 5513, Ecole Centrale de Lyon, 69134 Ecully, France

Edited by Federico Capasso, Harvard University, Cambridge, MA, and approved May 29, 2020 (received for review November 21, 2019)

A substantial challenge in guiding elastic waves is the presence of reflection and scattering at sharp edges, defects, and disorder. Recently, mechanical topological insulators have sought to overcome this challenge by supporting back-scattering resistant wave transmission. In this paper, we propose and experimentally demonstrate a reconfigurable electroacoustic topological insulator exhibiting an analog to the quantum valley Hall effect (QVHE). Using programmable switches, this phononic structure allows for rapid reconfiguration of domain walls and thus the ability to control back-scattering resistant wave propagation along dynamic interfaces for phonons lying in static and finite-frequency regimes. Accordingly, a graphene-like polyactic acid (PLA) layer serves as the host medium, equipped with periodically arranged and bonded piezoelectric (PZT) patches, resulting in two Dirac cones at the *K* points. The PZT patches are then connected to negative capacitance external circuits to break inversion symmetry and create nontrivial topologically protected bandgaps. As such, topologically protected interface waves are demonstrated numerically and validated experimentally for different predefined trajectories over a broad frequency range.

topological insulators | electroacoustic | piezoelectric | metamaterial

The need for lossless information carriers has generated increased interest in topologically protected structures in the past few years. The study of topological insulators (TIs) originated with electronic states in condensed matter physics (1–4), and they were later studied in electromagnetic materials (5–8). Recently, TIs have been investigated for phononic systems (elastic waves in solids) to control statical floppy modes (9–15) and dynamical edge waves (16, 17). These mechanical structures are induced by analogs to the quantum Hall (18), quantum spin Hall (19), or quantum valley Hall effects (QVHEs) (20) and inherently support topological edge states resistant to back-scattering at sharp interfaces, discrete defects, or continuous disorder (21, 22).

Mechanical TIs mimicking the quantum Hall effect require active means to break time-reversal symmetry (18, 23, 24) and have been achieved by using a weak magnetic field (25), by using gyroscopes or rotating frames (26–28), or by varying material properties in time and space (29–31). In contrast, mechanical TIs mimicking the quantum spin Hall effect (QSHE) (19, 21) may be achieved passively through breaking of spatial inversion symmetry. These TIs have been investigated numerically and tested experimentally for elastic waves in thin plates (22, 32, 33) and in discrete systems composed of masses and linear springs (15, 16, 19, 29). Compared to active TIs, they 1) do not require external energy input, 2) feature both forward- and backward-propagating edge modes, and 3) typically retain time-reversal symmetry (34).

A third approach for achieving a mechanical TI results from mimicking the QVHE, which breaks inversion symmetry in a simpler system. The QVHE was first predicted theoretically in graphene (35–37) and later observed in solid-state devices (38–40), photonic crystals (41–43), and graphene bilayers (44–46). Unlike QSHE, only one set of degenerate Dirac cones is required, which reduces the geometrical complexity of designing TIs for elastic media. Recently, QVHE has been extended to phononic systems to exhibit valley edge states (20) by using 1) anisotropic scatterers in sonic crystals (47) and 2) arrays of resonators or different inclusion types in thin plates (24, 48, 49).

Mechanical TIs proposed to date lack an easy means of reconfigurabilty, which is essential for enabling important TI-based applications. One potential means to overcome this issue, as explored in this paper, is to employ shunted piezoelectric (PZT) disks in which the system's mechanical impedance can be altered dramatically using negative capacitance circuits (50–52). Dynamic reconfigurability of such structures can then be obtained through simple on/off switching of these external circuits. By doing so, we propose and experimentally verify an electroacoustic TI which exhibits topologically protected edge states. This reconfigurable structure is composed of an elastic hexagonal lattice (made from polylactic acid [PLA] plastic) whose unit cell contains two shunted PZT disks, each connected to a negative capacitance circuit by an on/off switch. Closing one or the other circuit results in the breaking of mirror symmetry and yields mechanical behavior analogous to the QVHE.

Results

Graphene-Like Unit Cell. Fig. 1*A* displays the schematic of the unit cell composed of an $h_h = 0.5$ mm thick PLA layer, with

Significance

We present a demonstration of topologically protected states using reconfigurable electroacoustic TIs whose design is simple, effective, and straightforward to fabricate. Numerical simulations and experimental measurements illustrate topologically protected wave propagation, free of back-scattering, along edges and interfaces. We anticipate these materials will have broad implications for devices capable of mechanical logic and circuitry, which may have advantages over electronic equivalents in harsh operating conditions, or in replacing wireless systems near propagation dead zones. Due to their dynamic reconfigurability, they may also lead to small-scale multiplexing and demultiplexing devices for use in communication devices, similar to the ubiquitous surface acoustic wave (SAW) devices used to filter electromagnetic energy.

Author contributions: A.D., M.C., and M.J.L. designed research; A.D. performed research; M.J.L. supervised the research; A.D. contributed new reagents/analytic tools; A.D. analyzed data; and A.D. wrote the paper.

The authors declare no competing interest.

This article is a PNAS Direct Submission.

[1]To whom correspondence may be addressed. Email: michael.leamy@me.gatech.edu.

This article contains supporting information online at https://www.pnas.org/lookup/suppl/doi:10.1073/pnas.1920549117/-/DCSupplemental.

First published June 29, 2020.

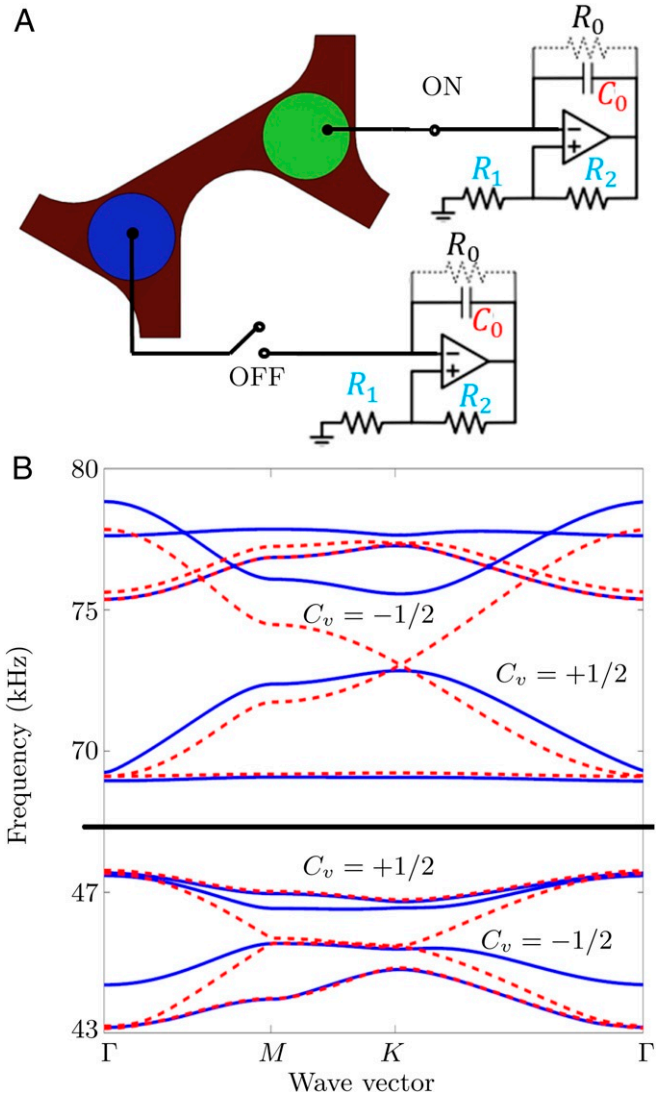

Fig. 1. Phononic crystal band structure. (*A*) Schematic of the phononic crystal formed by hexagonal unit cells with PLA ($h_0 = 0.5$ mm thick) as the host layer and attached circular PZT patches with thickness of $h_1 = 0.5$ mm ($d_1 = 7$ mm in diameter) connected to external circuits. These circuits provide negative capacitance of $C' = -(R_2 C_0)/R1$. (*B*) Comparison between the band structures in the absence (red dashed curves with two Dirac points at 45 and 73 kHz) and in the presence (blue solid curves with optimal bandgap at $C' = -1.7$ nF) of completed external circuits attached to one PZT disk.

two bonded PZT disks, used to mimic the band structure of graphene. This unit cell is then periodically repeated in the lattice directions to form the entire material system (see *SI Appendix*, Note 1, for more details). Each of the PZT disks employed has a diameter of 7 mm and a thickness of $h_p = 0.5$ mm and is connected to a negative capacitance circuit through a digital on/off switch. Red dashed lines in Fig. 1*B* plot the band structure of the unit cell when both of the switches are off (i.e., both of PZT disks experience open circuit conditions), documenting two Dirac cones at the edge of the unit cell where two distinct Lamb modes (53) meet (approximately $f_1 = 45$ kHz, $f_2 = 73$ kHz). Note that these curves are computed only for the frequency range of interest; hence, other Dirac cones are not visible. *SI Appendix*, Note 1, provides full discussion on the computation details for the entire frequency spectrum ($0 - 90$ kHz).

Breaking Inversion Symmetry. The next step in configuring the TI requires breaking mirror symmetry and separating the folded Dirac cones. As such, one of the switches in Fig. 1*B* is set to on, thus connecting the PZT (green disk) to the external negative capacitance circuit (Fig. 1*A*), which provides a significant change in the elastic modulus of the disk (51, 52, 54); the other PZT (blue disk) remains disconnected. This then enables breaking C_6 symmetry and creates a topological bandgap at the location of the Dirac cone. The circuit includes two resistors (R_1, R_2), one capacitor (C_0), and an operational amplifier, which yields an effective negative capacitance of $C' = -(R_2 C_0)/R_1$. Note that the resistor R_0 prevents saturation of the paralleled capacitance C_0, which can cause instability of the PZT disk. Blue solid lines in Fig. 1*B* plot the band structure of the described unit cell when the green PZT disk is connected in series with a negative capacitance of $C' = -1.7\ nF$, reporting two complete frequency bandgaps at the location of the Dirac modes. The stated negative capacitance is achieved by placing $R_1 = 10, R_2 = 17\ \Omega$ and $C_0 =$ 1nF, resulting in an optimal bandgap width. The band structures for other values of negative capacitance are provided in *SI Appendix*, Note 1.

For each of the bands bounding the topological gaps in Fig. 1*E*, the valley Chern numbers are computed numerically to be $C_v = \pm 1/2$ (as labeled on the graph). The computation of these numbers and the corresponding Berry curvatures are detailed in *SI Appendix*, Note 2. According to the bulk-edge correspondence principle (41, 55), for each of these bandgaps, the total Chern number is equal to the summation of the Chern numbers (ΔC_v) for all of the modes below the gap. If two structures with opposite total Chern numbers for bands share an interface (i.e., one structure with green disk shunted and the other with blue disk shunted), one U-shaped helical edge mode will be present at the interface ($|\Delta C_v| = 1$).

Topologically Protected Edge Waves. The most intriguing property of topological edge states is their ability to convey waves along sharp and curved interfaces without back-scattering. For QVHE, edge states are not present at the edge of the structure with a trivial mirror (e.g., air) since the difference in Chern numbers is less than one ($|\Delta C_{edge}| = \pm 1/2$); however, according to the bulk-edge correspondence principle (41, 55), if two materials with opposite Chern numbers share an interface ($|\Delta C_{interface}| = \pm 1$), topologically protected waves travel along this interface without losing their intensity. To verify these states in our system, a super cell composed of 10 unit cells in the y direction is considered (Fig. 2). This depicted strip is then repeated in the $x-$ direction by applying Bloch boundary conditions. As depicted in Fig. 2*B*, all of the green disks are electrically shunted, while the blue ones experience an open circuit condition. For the upper half of the super cell, locations of the green disks are reversed compared to the lower half, resulting in an interface with a Chern number difference of $|\Delta C_{interface}| = +1$. Fig. 2*A* documents the band structure of the super cell, revealing the existence of a topologically protected edge state starting from near the bulk modes on top to the bulk modes on the bottom at the location of the upper bandgap in Fig. 1*B*. Furthermore, the right schematic in Fig. 2*A* provides the displacement field of the strip at 73 kHz (marked with a red star). As observed, interface wave is localized at the interface.

Numerical Demonstration of Edge States. Next we report wave propagation immune to back-scattering along desired trajectories. For an ideal TI, data should travel along sharp and curved trajectories without loss of intensity. For mechanical TIs, this advantageous behavior has significant implications for communications systems, multiplexers, and onboard mechanical logic. To illustrate such a capability, a reconfigurable

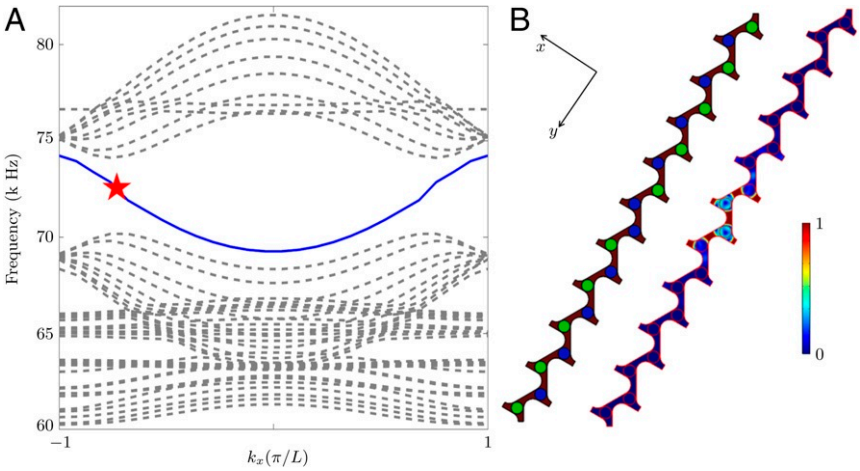

Fig. 2. Topologically protected interface state. (*A*) Band structure of a supercell composed of a 1-by-10 array of unit cells, periodically repeated in the *x* direction computed using Floquet boundary conditions. Gray curves depict bulk bands, while the blue curve depicts the protected interface mode. (*B*) (*Left*) Schematic of the supercell in which green disks are electrically shunted and blue ones are left open circuited, resulting in the upper half and lower half subdomains experiencing opposite Chern numbers. (*Right*) The corresponding wave distribution at a frequency of $f = 73$ kHz (marked with a red star), documenting wave localization at the interface. All displacements are normalized by the maximum deformation of the cell.

interface is created between two subdomains with opposite Chern numbers.

As such, we consider a plate composed of 8×8 hexagonal unit cells, each equipped with a pair of PZT disks. On one side of the interface the upper disks are shunted, while for the other side the lower ones are electrically shunted (or vice versa). Fig. 3*A* depicts the displacement field of the structure with a horizontal interface under a harmonic excitation at 73 kHz. As documented, waves clearly travel along the desired interface from the input (marked with the blue star) to the output (marked with the green star). As a second example, Fig. 3*B* displays an interface in which waves are guided along a triangular path from the source on the left side to the receiver on the bottom edge, without back-scattering or reflection at the sharp edges (again at 73 kHz). Finally, Fig. 3*C* depicts the displacement field for the case with a Z-shaped interface, documenting propagation with minimal intensity loss for 73 kHz. As desired, for all three interfaces, robustness of the system is guaranteed at the location of the interface.

Experimental Realization of Edge States. We next verify the performance of the proposed reconfigurable TI by carrying out a set of experiments. The experimental setup is composed of a 5×5 hexagonal array of unit cells incorporating 50 bonded PZT disks (see *SI Appendix*, Note 4, for full details on the experimental setup). Half of the PZT disks are connected to external circuits (by simply closing the attached switch) with an effective negative capacitance of $C' = -1.7$ nF to form an interface between two domains (marked with green line), one characterized by a valley Chern number $C_v = 1/2$ and the other by $C_v = -1/2$. Fig. 4*A* exhibits the experimentally measured RMS wavefield of a system with a horizontal interface in response to excitation at 77 kHz. This figure clearly confirms the propagation of an interface wave from the source (marked with a black star) to the receiver on the other side of the structure. Due to the imperfectness of the experimental setup and the mass and stiffness of the connected wires and soldering material, this frequency is slightly above that predicted using numerical simulations. As shown in Fig. 4*B*, the system is easily reconfigured to alter the interface location (at the same excitation frequency) simply by operation of the programmable on/off switches, in this case introducing a sharp-angled trajectory. An interface wave travels from the input on the left side to the output on the top edge with minimal reflections from the sharp geometry. For both trajectories appearing in Fig. 4, time snapshots of the interface wave traveling along the trajectories are provided in *SI Appendix*, Note 4.

Discussion

In summary, this paper presents a reconfigurable electroacoustic TI that realizes topological edge states analogous to the QVHE. The proposed phononic crystal is formed by periodically repeating a graphene-like unit cell, which is composed of two bonded PZT circular disks attached to a hexagonal PLA layer. In order to break inversion symmetry, one of the two disks is connected to an external circuit with negative

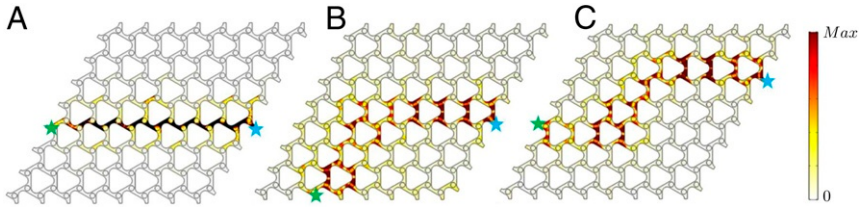

Fig. 3. Numerically computed interface waves. Numerically computed RMS displacement field of the system excited by a source (marked with blue stars) at 73 kHz, documenting back-scattering free wave propagation along (*A*) a horizontal interface, (*B*) a triangular-shaped interface, and (*C*) a Z-shaped interface. All displacements are normalized by the amplitude of the input wave. For these interfaces, the location of the shunted PZT patch on either side of the interface is reversed, providing $\Delta C_{interface} = \pm 1$ at the boundary of the two subdomains. Green stars depict the location of the wave output.

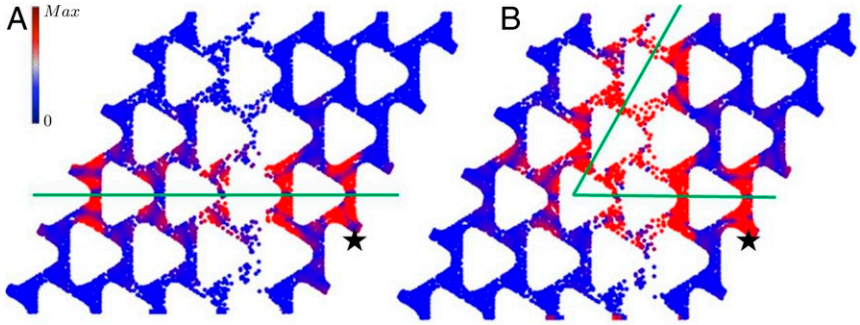

Fig. 4. Experimentally measured interface waves. Experimentally measured RMS displacement field of the system excited by a source (marked with black stars) at 77 kHz, documenting wave propagation (*A*) along a horizontal interface and (*B*) along a sharp-angled interface exhibiting back-scattering free propagation. Displacements are normalized by the amplitude of the input wave. For these interfaces, the location of the shunted PZT patch on either side of the green line is reversed.

capacitance, while the other one is left in an open circuit state. Dispersion relationships are computed numerically, documenting a topological bandgap at the location of the Dirac one. Numerically computed and experimentally measured results illustrate immune to back-scattering wave propagation along sharp interfaces. Furthermore, by simply operating on/off the desired circuits, reconfigurable interfaces are obtained and verified experimentally. The reconfigurable TI proposed in this study may be a stepping-stone material platform for implementing next generation acoustic-based wave filtering, multiplexing/demultiplexing, and logic in communication-based devices.

Data Availability.

All data needed to evaluate the conclusions in the paper are present in the paper and/or *SI Appendix*. Additional data related to this paper may be requested from the authors.

ACKNOWLEDGMENTS. We thank the National Science Foundation for supporting this research under Grant 1929849.

1. L. Lu, J. D. Joannopoulos, M. Soljačić, Topological photonics. *Nat. Photon.* **8**, 821–829 (2014).
2. M. Z. Hasan, C. L. Kane, Colloquium: Topological insulators. *Rev. Mod. Phys.* **82**, 3045 (2010).
3. K. Von Klitzing, The quantized hall effect. *Rev. Mod. Phys.* **58**, 519–531 (1986).
4. C. L. Kane, E. J. Mele, Quantum spin Hall effect in graphene. *Phys. Rev. Lett.* **95**, 226801 (2005).
5. F. Haldane, S. Raghu, Possible realization of directional optical waveguides in photonic crystals with broken time-reversal symmetry. *Phys. Rev. Lett.* **100**, 013904 (2008).
6. Z. Wang, Y. Chong, J. D. Joannopoulos, M. Soljačić, Reflection-free one-way edge modes in a gyromagnetic photonic crystal. *Phys. Rev. Lett.* **100**, 013905 (2008).
7. A. B. Khanikaev *et al.*, Photonic topological insulators. *Nat. Mater.* **12**, 233–239 (2013).
8. M. Hafezi, S. Mittal, J. Fan, A. Migdall, J. Taylor, Imaging topological edge states in silicon photonics. *Nat. Photon.* **7**, 1001–1005 (2013).
9. C. Kane, T. Lubensky, Topological boundary modes in isostatic lattices. *Nat. Phys.* **10**, 39–45 (2014).
10. J. Paulose, B. G.-g. Chen, V. Vitelli, Topological modes bound to dislocations in mechanical metamaterials. *Nat. Phys.* **11**, 153–156 (2015).
11. D. Z. Rocklin, B. G.-g. Chen, M. Falk, V. Vitelli, T. Lubensky, Mechanical Weyl modes in topological Maxwell lattices. *Phys. Rev. Lett.* **116**, 135503 (2016).
12. V. Vitelli, N. Upadhyaya, B. G.-g. Chen, Topological mechanisms as classical spinor fields. arXiv:1407.2890 (10 July 2014).
13. O. Stenull, C. Kane, T. Lubensky, Topological phonons and Weyl lines in three dimensions. *Phys. Rev. Lett.* **117**, 068001 (2016).
14. O. R. Bilal, R. Süsstrunk, C. Daraio, SD. Huber, Intrinsically polar elastic metamaterials. *Adv. Mater.* **29**, 1700540 (2017).
15. E. Prodan, K. Dobiszewski, A. Kanwal, J. Palmieri, C. Prodan, Dynamical majorana edge modes in a broad class of topological mechanical systems. *Nat. Commun.* **8**, 14587 (2017).
16. R. Süsstrunk, S. D. Huber, Observation of phononic helical edge states in a mechanical topological insulator. *Science* **349**, 47–50 (2015).
17. T. Kariyado, Y. Hatsugai, Manipulation of Dirac cones in mechanical graphene. *Sci. Rep.* **5**, 18107 (2015).
18. R. Fleury, D. L. Sounas, C. F. Sieck, M. R. Haberman, A. Alù, Sound isolation and giant linear nonreciprocity in a compact acoustic circulator. *Science* **343**, 516–519 (2014).
19. S. D. Huber, Topological mechanics. *Nat. Phys.* **12**, 621–623 (2016).
20. J. Lu, C. Qiu, M. Ke, Z. Liu, Valley vortex states in sonic crystals. *Phys. Rev. Lett.* **116**, 093901 (2016).
21. S. H. Mousavi, A. B. Khanikaev, Z. Wang, Topologically protected elastic waves in phononic metamaterials. *Nat. Commun.* **6**, 8682 (2015).
22. M. Miniaci, R. Pal, B. Morvan, M. Ruzzene, Experimental observation of topologically protected helical edge modes in patterned elastic plates. *Phys. Rev. X* **8**, 031074 (2018).
23. A. B. Khanikaev, R. Fleury, S. H. Mousavi, A. Alù, Topologically robust sound propagation in an angular-momentum-biased graphene-like resonator lattice. *Nat. Commun.* **6**, 8260 (2015).
24. J. Vila, R. K. Pal, M. Ruzzene, Observation of topological valley modes in an elastic hexagonal lattice. *Phys. Rev. B* **96**, 134307 (2017).
25. E. Prodan, C. Prodan, Topological phonon modes and their role in dynamic instability of microtubules. *Phys. Rev. Lett.* **103**, 248101 (2009).
26. Y. T. Wang, P. G. Luan, S. Zhang, Coriolis force induced topological order for classical mechanical vibrations. *New J. Phys.* **17**, 073031 (2015).
27. P. Wang, L. Lu, K. Bertoldi, Topological phononic crystals with one-way elastic edge waves. *Phys. Rev. Lett.* **115**, 104302 (2015).
28. L. M. Nash *et al.*, Topological mechanics of gyroscopic metamaterials. *Proc. Natl. Acad. Sci. U.S.A.* **112**, 14495–14500 (2015).
29. R. Chaunsali, E. Kim, A. Thakkar, P. G. Kevrekidis, J. Yang, Demonstrating an in situ topological band transition in cylindrical granular chains. *Phys. Rev. Lett.* **119**, 024301 (2017).
30. R. Fleury, A. B. Khanikaev, A. Alu, Floquet topological insulators for sound. *Nat. Commun.* **7**, 11744 (2016).
31. N. Swinteck *et al.*, Bulk elastic waves with unidirectional backscattering-immune topological states in a time-dependent superlattice. *J. Appl. Phys.* **118**, 063103 (2015).
32. R. Chaunsali, C. W. Chen, J. Yang, Subwavelength and directional control of flexural waves in zone-folding induced topological plates. *Phys. Rev. B* **97**, 054307 (2018).
33. C. He *et al.*, Topological phononic states of underwater sound based on coupled ring resonators. *Appl. Phys. Lett.* **108**, 031904 (2016).
34. L. D. Landau *et al.*, *Electrodynamics of Continuous Media* (Elsevier, 2013), **vol. 8**.
35. A. Rycerz, J. Tworzydo, C. Beenakker, Valley filter and valley valve in graphene. *Nat. Phys.* **3**, 172–175 (2007).
36. D. Xiao, W. Yao, Q. Niu, Valley-contrasting physics in graphene: Magnetic moment and topological transport. *Phys. Rev. Lett.* **99**, 236809 (2007).
37. F. Zhang, J. Jung, G. A. Fiete, Q. Niu, A. H. MacDonald, Spontaneous quantum hall states in chirally stacked few-layer graphene systems. *Phys. Rev. Lett.* **106**, 156801 (2011).
38. K. F. Mak, K. L. McGill, J. Park, P. L. McEuen, The valley Hall effect in MoS_2 transistors. *Science* **344**, 1489–1492 (2014).
39. R. Gorbachev *et al.*, Detecting topological currents in graphene superlattices. *Science* **346**, 448–451 (2014).
40. M. Sui *et al.*, Gate-tunable topological valley transport in bilayer graphene. *Nat. Phys.* **11**, 1027–1031 (2015).
41. T. Ma, G. Shvets, All-Si valley-Hall photonic topological insulator. *New J. Phys.* **18**, 025012 (2016).
42. J. W. Dong, X. D. Chen, H. Zhu, Y. Wang, X. Zhang, Valley photonic crystals for control of spin and topology. *Nat. Mater.* **16**, 298–302 (2017).
43. M. Xiao, W. J. Chen, W. Y. He, C. T. Chan, Synthetic gauge flux and Weyl points in acoustic systems. *Nat. Phys.* **11**, 920–924 (2015).
44. F. Zhang, A. H. MacDonald, E. J. Mele, Valley Chern numbers and boundary modes in gapped bilayer graphene. *Proc. Natl. Acad. Sci. U.S.A.* **110**, 10546–10551 (2013).
45. Y. Zhang *et al.*, Direct observation of a widely tunable bandgap in bilayer graphene. *Nature* **459**, 820–823 (2009).
46. L. Ju *et al.*, Topological valley transport at bilayer graphene domain walls. *Nature* **520**, 650–655 (2015).

47. J. Lu *et al.*, Observation of topological valley transport of sound in sonic crystals. *Nat. Phys.* **13**, 369–374 (2017).
48. R. K. Pal, M. Ruzzene, Edge waves in plates with resonators: An elastic analogue of the quantum valley Hall effect. *New J. Phys.* **19**, 025001 (2017).
49. A. Darabi, M. J. Leamy, Reconfigurable topological insulator for elastic waves. *J. Acoust. Soc. Am.* **146**, 773–781 (2019).
50. G. Trainiti *et al.*, Time-periodic stiffness modulation in elastic metamaterials for selective wave filtering: Theory and experiment. *Phys. Rev. Lett.* **122**, 124301 (2019).
51. S. Behrens, A. Fleming, S. Moheimani, A broadband controller for shunt piezoelectric damping of structural vibration. *Smart Mater. Struct.* **12**, 18–28 (2003).
52. B. S. Beck, K. A. Cunefare, M. Collet, The power output and efficiency of a negative capacitance shunt for vibration control of a flexural system. *Smart Mater. Struct.* **22**, 065009 (2013).
53. H. Lamb, On waves in an elastic plate. *Proc. R. Soc. Lond. A* **93**, 114–128 (1917).
54. N. W. Hagood, A. von Flotow, Damping of structural vibrations with piezoelectric materials and passive electrical networks. *J. Sound Vib.* **146**, 243–268 (1991).
55. B. I. Halperin, Quantized hall conductance, current-carrying edge states, and the existence of extended states in a two-dimensional disordered potential. *Phys. Rev. B* **25**, 2185–2190 (1982).